RESEARCH ARTICLE

RLC Circuit-based Detection of Subharmonics, Interharmonics, and Harmonics in Current and Voltage Waveforms

Mladen Banjanin[1,*] **and Bojana Čolić**[1]

[1] Faculty of Electrical Engineering, University of East Sarajevo, East Sarajevo 71123, Bosnia and Herzegovina

Abstract

This paper presents a simple and efficient method for detecting harmonics, interharmonics, and subharmonics in voltage and current waveforms. The proposed technique is based on a series RLC resonant circuit and is characterized by its simplicity, relatively fast response, and ease of implementation. The performance of the proposed method is validated using both mathematically generated signals with severe waveform distortion and signals measured in real distribution networks with high penetration of renewable energy sources. The maximum relative errors in the frequency of detected harmonic components were 1.33% for the mathematically generated strongly distorted signals and 0.60% for the measured signals. The relative errors in the estimated harmonic amplitudes, expressed with respect to the fundamental harmonic, were up to 4.75% for the strongly distorted mathematically generated signals and ranged from 1.28% to 11.75% for the measured signals. The errors decreased as the level of waveform distortion increased.

Keywords: harmonics, interharmonics, power quality, RLC circuit, subharmonics, waveform distortion.

1 Introduction

Modern electric power systems are characterized by significant integration of nonlinear loads and sources [1]. These components have a distorted current waveform, which, due to voltage drop on system impedances, distorts the voltage waveform. The harmonic spectrum of the distorted signals is mostly analyzed using different versions of the Fast Fourier Transform (FFT) [2]. However, FFT has an important limitation. It represents a distorted current or voltage waveform as a sum of sinusoidal functions whose frequencies are integer multiples of the fundamental frequency. This means that FFT cannot detect subharmonic components in the signal (whose frequency is lower than the fundamental frequency) or interharmonic components in the signal (whose frequency is a non-integer multiple of the fundamental frequency).

Interharmonics and subharmonics in voltage and current waveforms are primarily generated by strongly nonlinear and time-varying elements, such as variable speed drives, inverters used in renewable energy systems, controlled rectifiers, electric arc furnaces

Submitted: 06 June 2026
Revised: 18 August 2026
Accepted: 20 August 2026
Published: 01 September 2026

Vol. 2, **No.** 3, 2026.
10.62762/TEPNS.2026.598621

***Corresponding author:**
✉ Mladen Banjanin
mladen.banjanin@etf.ues.rs.ba

Citation
Banjanin, M., & Čolić, B. (2026). RLC Circuit-based Detection of Subharmonics, Interharmonics, and Harmonics in Current and Voltage Waveforms. *ICCK Transactions on Electric Power Networks and Systems*, 2(3), 128–137.

© 2026 ICCK (Institute of Central Computation and Knowledge)

and welding equipment, cycloconverters, doubly fed induction generators, etc. [3, 4]. Detection of the subharmonics and interharmonics in the signals is a complicated task, because it is necessary to detect that some subharmonic or interharmonic components do exist in the signal and it is necessary to calculate their parameters (amplitude, phase angle, etc.) [5]. Different methods are developed to detect subharmonic and interharmonic components in the signal [5–10]. In [6], a time-domain procedure for detecting harmonics and interharmonics is presented. The method is based on a high-resolution Prony algorithm combined with a down-sampling technique, enabling the precise resolution of closely spaced spectral components. In [7], an approach for interharmonic detection based on sparse signal decomposition using the Matching Pursuit algorithm and an overcomplete dictionary is proposed. The method is validated using both simulated and measured signals, demonstrating its effectiveness and robustness. In [8], a method based on multiple synchronous reference frame analysis is presented. By employing parallel computing techniques, the proposed approach enables real-time estimation of the amplitudes and phase angles of time-varying harmonics and interharmonics in rapidly fluctuating asymmetrical loads. In [9], a two-stage wavelet decomposition method is presented for evaluating instantaneous power quality indices. The approach combines customized filter banks and the Undecimated Wavelet Packet Transform, followed by the Hilbert transform, to analyze harmonic and interharmonic components. In [10], an FFT-based method for interharmonic detection is presented. The approach employs an interpolation FFT algorithm using the Blackman–Harris window together with the Rife–Vincent (I) and Rife–Vincent (III) windows to improve frequency estimation accuracy.

As demonstrated by the reviewed literature, numerous advanced methods have been developed for detecting harmonic spectra of the signal, including harmonic, interharmonic, and subharmonic components. These methods generally provide high detection accuracy, support real-time implementation, and enable accurate estimation of both the amplitudes and phase angles of spectral components. However, most of these techniques are computationally intensive, relatively complex to implement, and primarily intended for experts. Consequently, their implementation may present significant challenges for engineers, limiting their applicability in routine engineering tasks.

In many engineering applications, information about the phase angles of harmonic components in the signal is not required, nor is real-time estimation of the harmonic spectrum. Instead, it is often sufficient to identify the presence and approximate frequencies and amplitudes of significant harmonics, interharmonics, and subharmonics. Such information is essential for avoiding resonance conditions in the design of electrical networks and loads, when selecting appropriate harmonic filters, assessing power quality, etc. Therefore, engineers often require methods that are simple, fast, reliable, and easy to implement, while providing a clear identification of the significant spectral components without the need for highly accurate calculation of their amplitudes and phase angles.

This paper presents an RLC resonant circuit-based method for detecting subharmonics, interharmonics, and harmonics in current and voltage waveforms. The proposed method is validated using both strongly distorted mathematically generated signals and signals measured in a real distribution network with renewable energy sources. Compared to the FFT-based analysis, whose performance is limited to detecting harmonic components in the signal, the proposed method enables detection of harmonic, interharmonic, and subharmonic components. Consequently, it provides more comprehensive information about the spectral content of voltage and current signals. The presented method is simple and can be easily implemented by engineers who are not experts in the field of signal processing and harmonic spectra calculation.

The paper is organized as follows: Section 2 describes the proposed method for detecting subharmonics, interharmonics, and harmonics in current and voltage signals; Section 3 presents the calculation results, including those obtained from mathematically generated highly distorted signals (Section 3.1) and from signals measured at the points of common coupling (PCCs) of photovoltaic (PV) power plants in real distribution networks (Section 3.2); and finally, Section 4 concludes the paper by summarizing the main findings, discussing the proposed method, and outlining directions for future research.

2 Description of the applied method for the detection of subharmonics, interharmonics, and harmonics in the signal

The presented approach of detecting subharmonics, interharmonics, and harmonics in the voltage or

current waveforms is based on the application of a series-resonant RLC circuit shown in Figure 1. The voltage balance equation for the circuit presented in Figure 1 is defined by equation (1):

$$u_s(t) = R \cdot i(t) + L\frac{di(t)}{dt} + \frac{1}{C}\int i(t)\,dt \qquad (1)$$

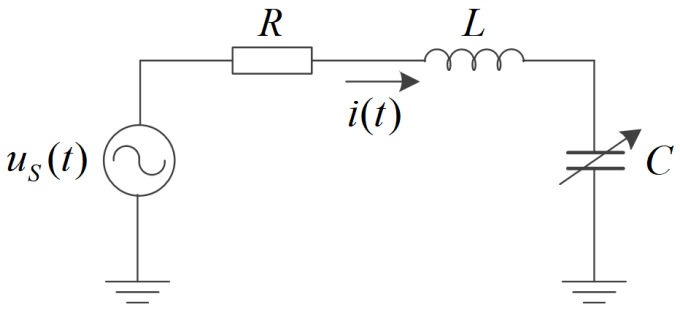

Figure 1. Series-resonant RLC circuit used to detect subharmonics, interharmonics, and harmonics in the voltage and current waveforms.

The detection procedure can be summarized as follows:

1) Generate a mathematical signal for analysis or measure it in a real network.

2) Use samples of the signal (current or voltage) from the previous step to implement the voltage source $u_s(t)$ in Figure 1.

3) Use the following values of the RLC parameters:

   a. R should be low to achieve a high Q factor of the series RLC circuit, equation (2). A high Q factor of a series RLC circuit indicates sharp resonant peaks and a narrow bandwidth of the circuit, which is essential for highly selective band-pass filters. This enables good detection efficiency of harmonic components, especially if there are close harmonic components in a signal. However, too high a Q factor can lead to numerical instability. $R = 0.1\ \Omega$ is applied.

$$\left.\begin{aligned} Q &= \frac{1}{R}\sqrt{\frac{L}{C}}, \\ \omega_r &= \sqrt{\frac{1}{LC}} \end{aligned}\right\} \Rightarrow Q = \frac{\omega_r L}{R} = \frac{2\pi f_r L}{R} \qquad (2)$$

   b. L is assumed to be 0.1 H to keep a high value of the Q factor even at the low frequencies (f_r), equation (2). The values of R and L can vary over a wide range, without significantly affecting calculated results.

   c. C is calculated using equation (3). It is varied in such a way that the resonance frequency of the series RLC circuit is in the range $f_1 \leq f_r \leq f_2$. In this paper, $0 \leq f_r \leq 600$ Hz is applied (but in some cases $0 \leq f_r \leq 250$ Hz or $0 \leq f_r \leq 300$ Hz). The DC component in a signal can be accurately calculated as the mean signal value. The presented approach always gives some DC component, and the explanation is as follows: equation (3), for the DC signal, gives an infinite value of capacitance C, consequently, MATLAB converts a capacitor into a short circuit, leaving a low resistance series RL circuit with large time constant, consequently, some DC decaying current exist in the current i(t) from Figure 1.

$$C = \frac{1}{L(2\pi f_r)^2} \qquad (3)$$

4) Numerically solve equation (1) using the `ode45` solver in MATLAB. The solution provides the current $i(t)$ corresponding to the circuit shown in Figure 1.

5) The RMS value of the current $i(t)$ is calculated based on the samples from the last 20% of the signal when the transient process in the RLC circuit is more damped. A longer time calculation enables a more accurate calculation of the signal spectra.

6) Present calculated results.

All analyses and simulations presented in this paper were performed on a desktop PC equipped with an Intel® Core™ i5-12400 (12th Gen) processor (6 cores, 12 threads, up to 4.4 GHz), 32 GB of DDR4-3200 RAM, an MSI PRO H610M-E DDR4 (MS-7D48) motherboard, and a 477 GB SSD. The duration of calculations was up to a few minutes, depending on the considered frequency range, adopted frequency step, and analyzed signal duration. The proposed method can also be executed on less powerful PCs but with a longer simulation time.

3 Results of Calculations

3.1 Mathematically Generated Signals

The presented method of harmonics, subharmonics, and interharmonics detection is applied to strongly distorted mathematically generated signals. Phase angles of harmonic components are varied to assess the method's accuracy and applicability under different conditions.

Table 1. Mathematically generated signals in Case 1.

Harmonic components in the signal	0 Hz DC	50 Hz 1st harmonic	150 Hz 3rd harmonic	250 Hz 5th harmonic	350 Hz 7th harmonic	550 Hz 11th harmonic
Amplitude [p.u.] (signals 1 and 2)	0.1	1	0.2	0.5	0.35	0.15
Phase angle [rad] (signal 1)	–	0	0	0	0	0
Phase angle [rad] (signal 2)	–	$\pi/4$	$2\pi/4$	$3\pi/4$	$5\pi/4$	$6\pi/4$

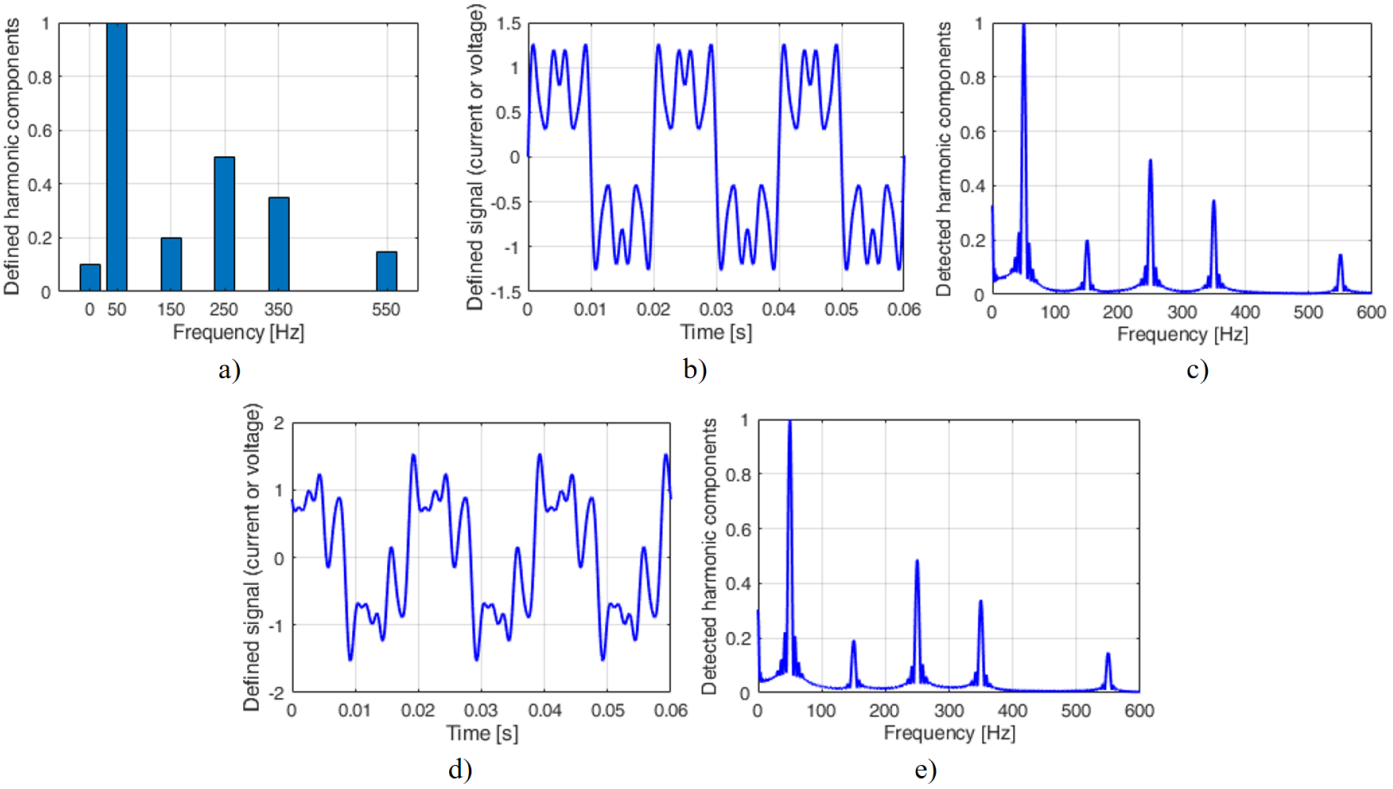

Figure 2. a) Defined harmonic components in the signal, b) waveform of signal 1, c) calculated harmonic spectra of signal 1, d) waveform of signal 2, e) calculated harmonic spectra of signal 2.

Table 2. Comparison of the defined and detected frequencies of the spectral components in signals 1 and 2.

Defined harmonics in signals 1 and 2	0 Hz DC	50 Hz 1st harmonic	150 Hz 3rd harmonic	250 Hz 5th harmonic	350 Hz 7th harmonic	550 Hz 11th harmonic
Detected harmonics in signal 1	0 Hz	50.0 Hz	149.9 Hz	249.9 Hz	350.0 Hz	549.9 Hz
Detected harmonics in signal 2	0 Hz	49.9 Hz	150.4 Hz	250 Hz	349.9 Hz	549.8 Hz
Relative error, signal 1	0	0.00%	-0.07%	-0.04%	0.00%	-0.02%
Relative error, signal 2	0	-0.20%	0.27%	0.00%	-0.03%	-0.04%

Table 3. Comparison of the defined and estimated relative amplitudes of the spectral components in signals 1 and 2.

Defined harmonics in signals 1 and 2	0 Hz DC	50 Hz 1st harmonic	150 Hz 3rd harmonic	250 Hz 5th harmonic	350 Hz 7th harmonic	550 Hz 11th harmonic
Defined amplitude [p.u.] (signals 1 and 2)	0.1	1	0.2	0.5	0.35	0.15
Calculated amplitude [p.u.] (signal 1)	0.1	1	0.200	0.496	0.347	0.148
Calculated amplitude [p.u.] (signal 2)	0.1	1	0.194	0.493	0.343	0.149
Relative error, signal 1	0%	–	-0.11%	-0.72%	-0.87%	-1.09%
Relative error, signal 2	0%	–	-2.77%	-1.39%	-1.90%	-0.76%

Case 1 – signal with the DC component and 1st, 3rd, 5th, 7th, and 11th harmonics

The signals 1 and 2 used in Case 1 are defined in Table 1. The same harmonic amplitudes are applied in signals 1 and 2, but with different phase angles. Calculated results are presented in Figure 2. It can be noticed that all harmonic components in the signal are well detected. The duration of the calculations was 0.2 s, while in Figure 2(b) and Figure 2(d), only a

0.06 s period is presented to improve figure readability. The duration of the simulation is a very important parameter because a longer simulation enables the RLC circuit to reach a steady-state condition and to calculate the harmonic spectra more accurately. Comparisons between the defined and calculated harmonic spectra of the signals from Table 1 and Figure 2 are given in Table 2. Relative errors in the calculated results are low, up to 0.27%, and can be even smaller in a longer simulation. Comparisons of the defined and calculated harmonic amplitudes of the signals from Table 1 and Figure 2 are given in Table 3. Relative errors in the calculated results are low, up to -2.77%. DC component in the signal can be calculated as the mean signal value, Table 3. Calculation of harmonic amplitudes is done relative to the 1st harmonic (50 Hz), which represents 1 per unit (p.u.).

Relative error (RE) of calculated results (CR) compared to the accurate results (AR) is calculated using equation (4):

$$RE = \frac{CR - AR}{AR} \cdot 100\% \tag{4}$$

The dependence of the current [i(t)] waveform on the resonant frequency of the RLC circuit (Figure 1) and on the simulation duration for signal 1 is illustrated in Figure 3. If the simulation duration is 0.06 s, current waveforms and amplitudes are very similar for resonant frequencies of the RLC circuit equal to 50 Hz and 55 Hz, as illustrated in Figure 3(a) and Figure (c). This leads to the low accuracy of calculated results. However, if simulation duration is increased to 0.2 s current waveforms are completely different for the same resonant frequencies equal to 50 Hz and 55 Hz, as illustrated in Figure 3(b) and Figure 3(d). Because of that, in the case of strongly distorted signals, such as signal 1, longer simulation time may be required to enable circuit current (i(t) in Figure 1) to reach values that enable reliable spectrum estimation.

Case 2 – signal with DC component, 17 Hz subharmonic, 120 Hz interharmonic, and 1st, 3rd, and 5th harmonics

The signals 3 and 4 used in Case 2 are defined in Table 4. The same amplitudes of the subharmonic, interharmonic, and harmonics are applied in signals 3 and 4, but with different phase angles. Calculated results are presented in Figure 4. The duration of the calculations was 0.4 s. All defined subharmonic, interharmonic and harmonic components in the signal are well detected. Comparisons of the defined and calculated harmonic spectra of the signals from Table 4 and Figure 4 are given in Table 5. The relative errors range from -1.76% to 0%, which is very accurate for such a distorted signal and for engineering practice. In longer simulations, errors will be additionally reduced. Comparisons of the defined and calculated harmonic amplitudes of the signals from Table 4 and Figure 4 are given in Table 6. Relative errors in the calculated results are up to 4.75%. DC component in the signal can be calculated as the mean signal value, Table 6. Calculation of harmonic amplitudes in Table 6 is done relative to the 1st harmonic (50 Hz), which represents 1 p.u.

Case 3 – signal with 15 Hz subharmonic and 75 Hz and 180 Hz interharmonics

Signal 5, used in Case 3, is defined in Table 7. Calculated results are presented in Figure 5. All harmonic components in the signal are well detected. Comparisons of the defined and calculated harmonic spectra of the signals from Table 7 and Figure 5 are given in Table 8. Relative errors in the calculated results are up to 1.33%, which is very good for engineering practice and can be additionally reduced in a longer simulation. Comparisons of the defined and calculated harmonic amplitudes of the signal from Table 7 and Figure 5 are given in Table 9. Relative errors in the calculated results are up to 4.62%. Calculation of harmonic amplitudes in Table 9 is done relative to the 15 Hz subharmonic, which represents 1 p.u.

3.2 Signals measured in real distribution networks

The presented method of subharmonics, harmonics, and interharmonics detection is applied to signals measured in real distribution networks [2, 11]. Distorted current signals measured at the PCC of the PV power plants connected to 0.4 kV distribution networks are used.

Calculated results for signals 6, 7 and 8 are presented in Figures 6, 7 and 8, respectively. Calculations are made using the standard FFT and the suggested method. Comparisons of calculated results are given in Tables 10 and 11. All harmonic components in the signal are detected with high accuracy, even for the relatively short simulation duration of 0.08 s. Relative errors of calculated results in Table 10 are up to 0.6%. The high accuracy of detected signal harmonic spectra proves that the presented method is applicable in real-world situations and in the presence of signal noise. Comparisons of the harmonic amplitudes calculated using the FFT and the presented method for

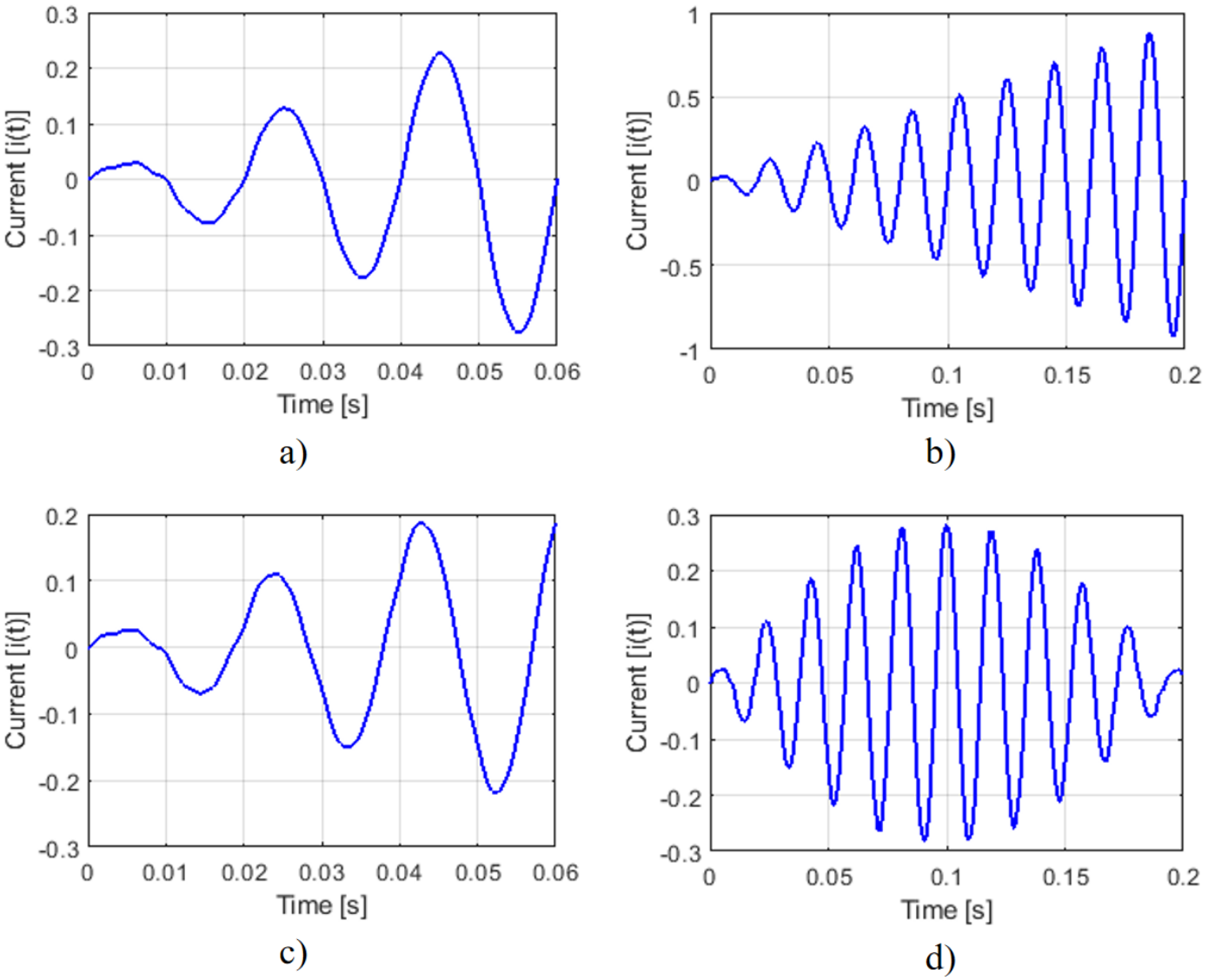

Figure 3. Waveform of the current i(t) from Figure 1 at the resonant frequency of the RLC circuit and simulation duration respectively equal to: a) 50 Hz and 0.06 s, b) 50 Hz and 0.2 s, c) 55 Hz and 0.06 s, d) 55 Hz and 0.2 s.

Table 4. Mathematically generated signals in Case 2.

Harmonic components in the signals 3 and 4	0 Hz DC	17 Hz subharmonic	50 Hz 1st harmonic	120 Hz interharmonic	150 Hz 3rd harmonic	250 Hz 5th harmonic
Amplitude [p.u.] (signals 3 and 4)	0.1	0.15	1	0.2	0.3	0.4
Phase angle [rad] (signal 3)	–	0	0	0	0	0
Phase angle [rad] (signal 4)	–	$\pi/4$	$2\pi/4$	$3\pi/4$	$5\pi/4$	$6\pi/4$

Table 5. Comparison of the defined and detected frequencies of the spectral components in signals 3 and 4.

Defined harmonics in signals 3 and 4	0 Hz DC	17 Hz subharmonic	50 Hz 1st harmonic	120 Hz interharmonic	150 Hz 3rd harmonic	250 Hz 5th harmonic
Detected harmonics in signal 3	0 Hz	16.7 Hz	49.9 Hz	119.9 Hz	150 Hz	250 Hz
Detected harmonics in signal 4	0 Hz	16.9 Hz	50.0 Hz	120.0 Hz	149.9 Hz	249.9 Hz
Relative error, signal 3	0	-1.76%	-0.20%	-0.08%	0.00%	0.00%
Relative error, signal 4	0	-0.59%	0.00%	0.00%	-0.07%	-0.04%

the signals from Figures 6, 7 and 8 are given in Table 11. The relative errors obtained in this case are significantly higher than those reported in Table 10, reaching 1.95% for Signal 6, 3.61% for Signal 7, and 11.75% for Signal 8. The errors decrease as the amplitudes of the higher-order harmonics become more pronounced

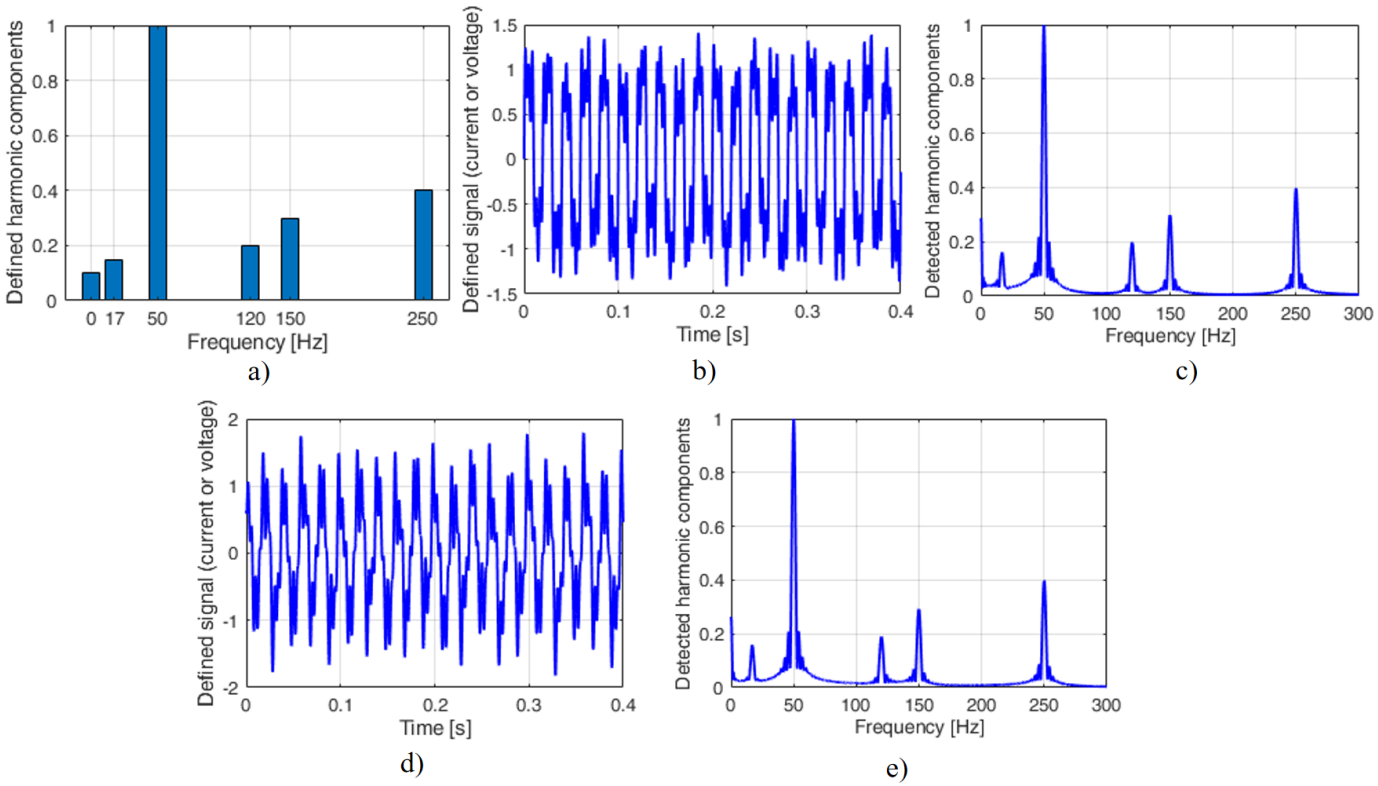

Figure 4. a) Defined harmonic components in the signal, b) waveform of signal 3, c) calculated harmonic spectra of signal 3, d) waveform of signal 4, e) calculated harmonic spectra of signal 4.

Table 6. Comparison of the defined and estimated relative amplitudes of the spectral components in signals 3 and 4.

Defined harmonics in signals 3 and 4	0 Hz DC	17 Hz subharmonic	50 Hz 1st harmonic	120 Hz interharmonic	150 Hz 3rd harmonic	250 Hz 5th harmonic
Defined amplitude [p.u.] (signals 3 and 4)	0.1	0.15	1	0.2	0.3	0.4
Calculated amplitude [p.u.] (signal 3)	0.1	0.157	1	0.198	0.299	0.398
Calculated amplitude [p.u.] (signal 4)	0.1	0.156	1	0.191	0.292	0.398
Relative error, signal 3	0%	4.75%	–	-0.81%	-0.46%	-0.60%
Relative error, signal 4	0%	3.90%	–	-4.73%	-2.55%	-0.43%

Table 7. Mathematically generated signal in Case 3.

Harmonic components in the signal 5	15 Hz subharmonic	75 Hz interharmonic	180 Hz interharmonic
Amplitude [p.u.]	1	0.2	0.5
Phase angle [rad]	$\pi/4$	$2\pi/4$	$3\pi/4$

Table 8. Comparison of the defined and detected frequencies of the spectral components in signal 5.

Defined harmonics in signal 5	15 Hz subharmonic	75 Hz interharmonic	180 Hz interharmonic
Detected harmonics in signal 5	15.2 Hz	75.1 Hz	180 Hz
Relative error, signal 5	1.33%	0.13%	0.00%

Table 9. Comparison of the defined and estimated relative amplitudes of the spectral components in signal 5.

Defined harmonics in signal 5	15 Hz subharmonic	75 Hz interharmonic	180 Hz interharmonic
Defined amplitude [p.u.] (signal 5)	1	0.2	0.5
Calculated amplitude [p.u.] (signal 5)	1	0.208	0.523
Relative error, signal 5	–	4.07%	4.62%

Table 10. Comparison of the frequencies of the spectral components detected using the proposed method and the standard FFT for signals 6, 7, and 8.

Standard FFT	50 Hz	250 Hz	350 Hz	550 Hz
Suggested method, signal 6	50.2 Hz	251 Hz	351.3 Hz	552 Hz
Suggested method, signal 7	50.1 Hz	250.8 Hz	351.5 Hz	551.9 Hz
Suggested method, signal 8	50.3 Hz	249.4 Hz	351.6 Hz	–
Relative error, signal 6	0.40%	0.40%	0.37%	0.36%
Relative error, signal 7	0.20%	0.32%	0.43%	0.35%
Relative error, signal 8	0.60%	-0.24%	0.46%	–

Table 11. Comparison of the relative amplitudes of the spectral components obtained using the proposed method and the standard FFT for signals 6, 7, and 8.

Harmonic component	50 Hz	250 Hz	350 Hz	550 Hz
Standard FFT (signal 6) [p.u.]	1	0.383	0.138	0.133
Standard FFT (signal 7) [p.u.]	1	0.196	0.073	0.043
Standard FFT (signal 8) [p.u.]	1	0.0325	0.0434	–
Calculated amplitude [p.u.] (signal 6)	1	0.378	0.135	0.131
Calculated amplitude [p.u.] (signal 7)	1	0.189	0.071	0.044
Calculated amplitude [p.u.] (signal 8)	1	0.0304	0.0383	–
Relative error, signal 6	–	-1.28%	-1.92%	-1.95%
Relative error, signal 7	–	-3.30%	-3.61%	3.14%
Relative error, signal 8	–	-6.31%	-11.75%	–

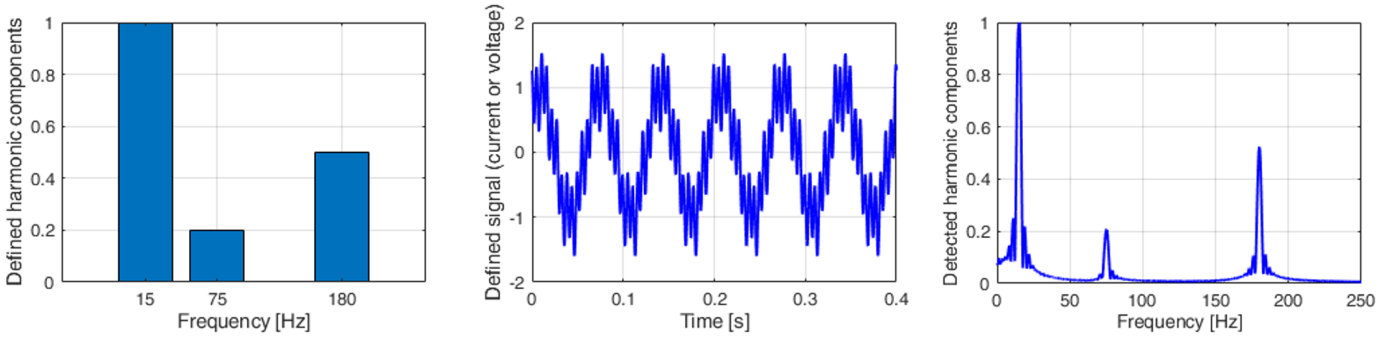

Figure 5. a) Defined harmonic components in the signal, b) waveform of signal 5, c) calculated harmonic spectra of signal 5.

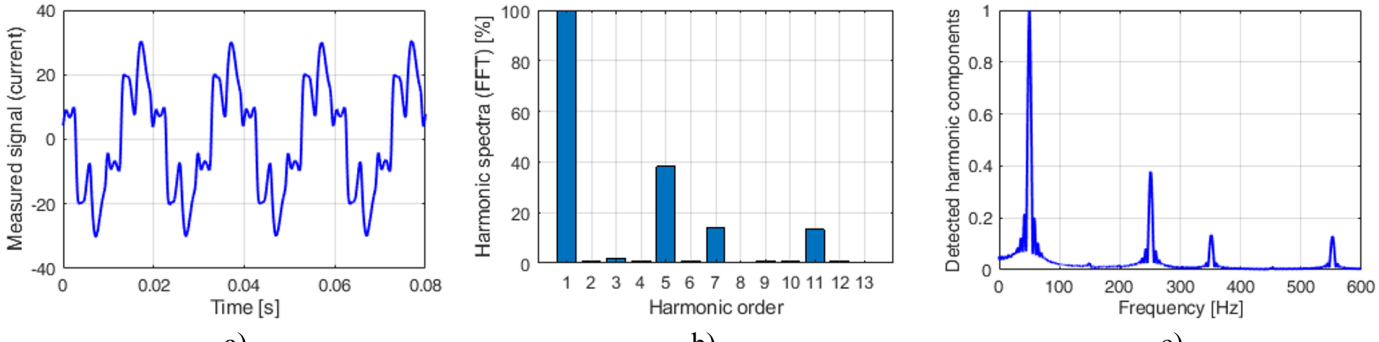

Figure 6. a) Measured signal 6, b) harmonic spectra of signal 6 (FFT), c) detected harmonic spectra of signal 6.

relative to the fundamental component, i.e., for more heavily distorted signals. The harmonic amplitudes presented in Table 11 are expressed relative to the fundamental harmonic (50 Hz), which is taken as 1

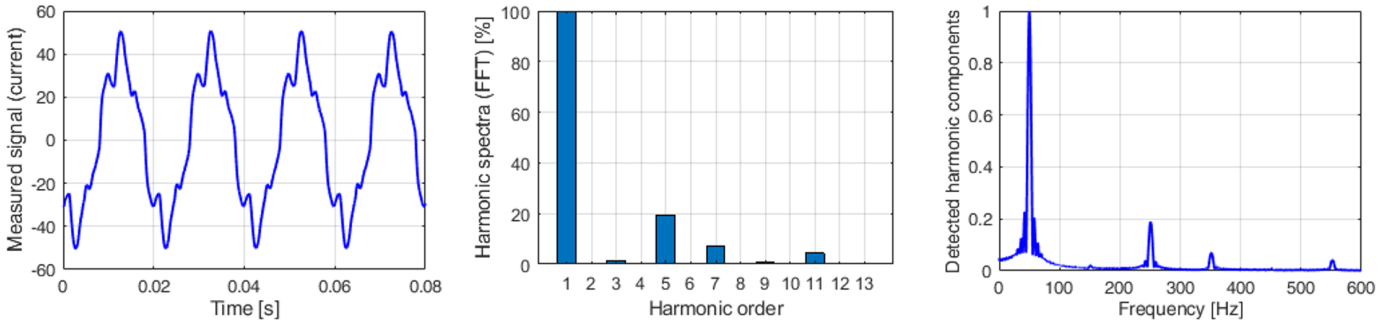

Figure 7. a) Measured signal 7, b) harmonic spectra of signal 7 (FFT), c) detected harmonic spectra of signal 7.

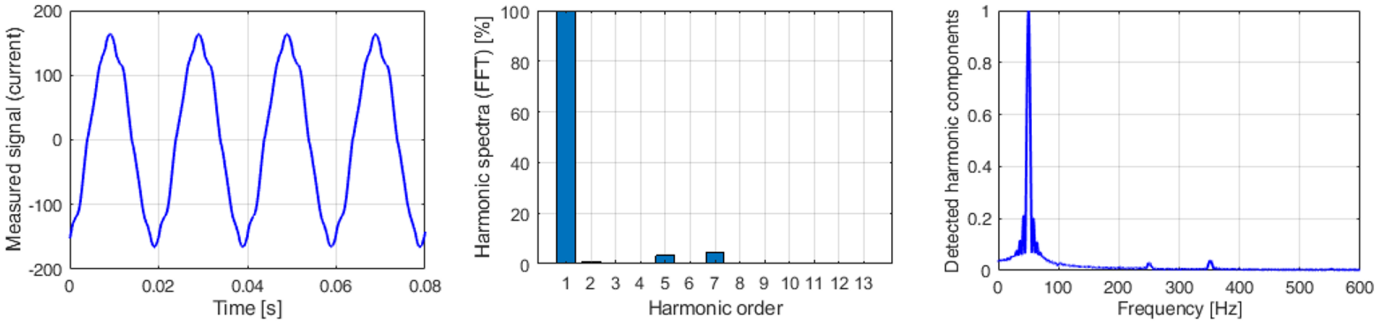

Figure 8. a) Measured signal 8, b) harmonic spectra of signal 8 (FFT), c) detected harmonic spectra of signal 8.

p.u.

4 Conclusion

The proposed method for determining the harmonic spectra of voltage and current waveforms, including the DC component, subharmonics, harmonics, and interharmonics, is accurate, relatively fast, and straightforward to implement. The accuracy and applicability of the method have been validated using both strongly distorted mathematically generated signals and signals measured in a real 0.4-kV distribution network at the PCCs of PV power plants. The proposed method identifies the presence of subharmonics, interharmonics, and harmonic components in the signal and determines their amplitudes relative to a selected reference harmonic, which is typically fundamental (50 Hz). In its current form, the proposed method does not provide accurate estimates of harmonic amplitudes in absolute values or their corresponding phase angles. The accuracy of the calculated relative harmonic amplitudes increases as the level of waveform distortion increases. The method is not yet sufficiently fast for real-time applications, because the calculations required up to a few minutes. Nevertheless, computational time strongly depends on the analyzed frequency range, the selected frequency resolution, the duration of the analyzed signal, and the computational performance of the hardware. Consequently, analyses over a limited frequency range, using shorter signal records and larger frequency steps, can be performed within a relatively short time. Future work will focus on extending the proposed method to enable real-time analysis of dynamically varying signals containing subharmonics, harmonics and interharmonics. In addition, methods for accurately estimating the absolute amplitudes and phase angles of subharmonic, interharmonic, and harmonic components will be investigated. Further research will also examine the influence of signal noise and waveform distortion on the accuracy of harmonic spectrum estimation. Finally, comparisons with other subharmonics, harmonics and interharmonics detection methods will be made.

Data Availability Statement

Data will be made available on request.

Funding

This work was supported without any funding.

Conflicts of Interest

Mladen Banjanin served as an Associate Editor of the *ICCK Transactions on Electric Power Networks and Systems*

at the time of manuscript submission. To ensure the integrity of the peer-review process, Mladen Banjanin was not involved in the editorial handling, peer review, or decision-making process for this manuscript, which was handled independently by another editor. The remaining authors declare no conflicts of interest.

AI Use Statement

The authors declare that no generative AI was used in the preparation of this manuscript.

Ethical Approval and Consent to Participate

Not applicable.

References

[1] Banjanin, M., Vuković, G., Erceg, B., Perović, B., & Milovanović, M. (2025). Power Quality of the 50 MW PV Power Plant. *ICCK Transactions on Electric Power Networks and Systems, 1*(2), 58-69. [CrossRef]

[2] Banjanin, M., Ikić, M., Milovanović, M., & Perović, B. (2025). Harmonic Analysis of Distributed Energy Sources Using Sliding FFT and IEC 61000-4-7. *Revue Roumaine des Sciences Techniques, Série Électrotechnique et Énergétique, 70*(4), 507–512. [CrossRef]

[3] Lin, H. C. (2014). Sources, effects, and modelling of interharmonics. *Mathematical Problems in Engineering, 2014*(1), 730362. [CrossRef]

[4] Testa, A., Akram, M. F., Burch, R., Carpinelli, G., Chang, G., Dinavahi, V., ... & Xu, W. (2007). Interharmonics: Theory and modeling. *IEEE Transactions on Power Delivery, 22*(4), 2335-2348. [CrossRef]

[5] Li, C., Xu, W., & Tayjasanant, T. (2003). Interharmonics: basic concepts and techniques for their detection and measurement. *Electric Power Systems Research, 66*(1), 39-48. [CrossRef]

[6] Chang, G. W., & Chen, C. I. (2009). An accurate time-domain procedure for harmonics and interharmonics detection. *IEEE transactions on power delivery, 25*(3), 1787-1795. [CrossRef]

[7] Li, Y., Teng, Z., Tang, Q., & Ji, Z. (2021). Detection of interharmonics using sparse signal decomposition based on ICA-MP. *IEEE Transactions on Instrumentation and Measurement, 70*, 1-9. [CrossRef]

[8] Uz-Logoglu, E., Salor, O., & Ermis, M. (2019). Real-time detection of interharmonics and harmonics of AC electric arc furnaces on GPU framework. *IEEE Transactions on Industry Applications, 55*(6), 6613-6623. [CrossRef]

[9] Yu, Y., Zhao, W., Li, S., & Huang, S. (2021). A two-stage wavelet decomposition method for instantaneous power quality indices estimation considering interharmonics and transient disturbances. *IEEE Transactions on Instrumentation and Measurement, 70*, 1-13. [CrossRef]

[10] Qian, H., Zhao, R., & Chen, T. (2007). Interharmonics analysis based on interpolating windowed FFT algorithm. *IEEE Transactions on Power Delivery, 22*(2), 1064-1069. [CrossRef]

[11] Banjanin, M., Milovanović, M., & Radosavljević, J. (2025). Voltage dips and swells detection by sliding fast Fourier transform: Possibilities for application in modern distribution networks. *Journal of Electrical Engineering, 76*(1), 58-71. [CrossRef]

Mladen Banjanin was born in Sarajevo, Yugoslavia, in 1988. He received his BSc degree in 2011 from the Faculty of Electrical Engineering, University of East Sarajevo, Bosnia and Herzegovina, and MSc and PhD degrees in 2012 and 2017, respectively, from the School of Electrical Engineering, University of Belgrade, Serbia. He is an associate professor at the Faculty of Electrical Engineering, University of East Sarajevo, and a visiting professor at the Faculty of Electrical Engineering, University of Banja Luka. His main areas of interest include lightning protection, high-voltage engineering, grounding systems, and power quality. (Email: mladen.banjanin@etf.ues.rs.ba)

Bojana Čolić was born in Foča, former Yugoslavia, in 1984. She received the BSc and MSc degrees from the Faculty of Electrical Engineering, University of East Sarajevo, Bosnia and Herzegovina, in 2009 and 2010, respectively. She is currently pursuing PhD degree at the School of Electrical Engineering, University of Belgrade, Serbia. She is a teaching assistant at the Faculty of Electrical Engineering, University of East Sarajevo. Her research interests include high voltage engineering, power factor correction, and power quality. (Email: bojana.novakovic@etf.ues.rs.ba)